ACS Macro Letters

Letter

pubs.acs.org/macroletters

Evolution of Chain Conformation and Entanglements during Startup Shear

Yuyuan Lu,[†] Lijia An,*[,†] Shi-Qing Wang,*[,‡] and Zhen-Gang Wang*[,§]

[†]State Key Laboratory of Polymer Physics and Chemistry, Changchun Institute of Applied Chemistry, Chinese Academy of Sciences, Changchun 130022, P.R. China

[‡]Department of Polymer Science, University of Akron, Akron, Ohio 44325-3909, United States

[§]Division of Chemistry and Chemical Engineering, California Institute of Technology, Pasadena, California 91125, United States

Supporting Information

ABSTRACT: Using Brownian dynamics simulation, we determine chain dimensions in an entangled polymer melt undergoing startup shear at a rate lower than the reciprocal of the Rouse time yet higher than the reciprocal reptation time. Here the tube model expects negligible chain stretching. In contrast, our simulation shows the deformed coil to conform closely to affine deformation. We find that the total number of entanglements decreases with increasing shear. Remarkably, up to many Rouse time, the decline in the number of initial entanglements is slower than that under the quiescent condition. These results point to fundamental deficiencies in the molecular picture of the tube model for startup shear.

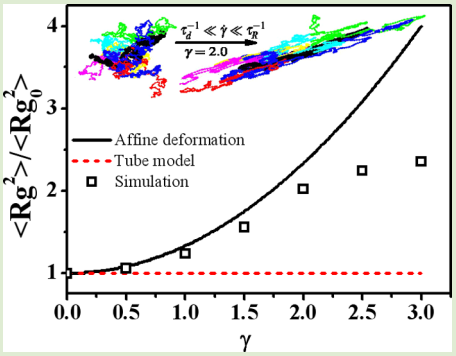

Characterizing chain entanglement in concentrated solutions and melts of long polymers and elucidating its dynamic evolution under external deformation are some of the greatest challenges in polymer physics.[1−5] Many theoretical attempts have been made in the past,[6−9] and the reptation-tube theory has emerged as the most widely accepted model to characterize linear viscoelastic properties as well as nonlinear rheological behavior of entangled polymers.[6−9] The concept of tube-like confinement has also been extended to treat dynamics of entangled semiflexible chains.[10] The tube model simplifies the complex, many-body effects of molecular interpenetration in terms of a smooth tube-like confinement on a test chain. By construction, the intermolecular interaction of the test chain with the surrounding chains is reduced to its frictional contact with the fictitious tube. Free of entanglement inside the tube, the test chain is assumed to execute Rouse dynamics.[11] Predictions of the tube model for equilibrium dynamics and linear rheological properties appear to be consistent with experiment.[12,13] Moreover, the existence of a confining tube along with its attributes as envisioned by the tube model has been supported by computer simulation.[14−18]

The physical basis for extending the tube model to large deformation is less obvious. Since the tube model does not describe how chain entanglement arises, it cannot address the question of when, how, and why disentanglement may occur due to fast external deformation. While a number of the predictions of the tube model, such as the stress overshoot in startup shear and strain softening after a large step shear, are in apparent agreement with macroscopic rheological measurements, several authors have raised questions about the microscopic foundation of the tube model.[19−21] More importantly, particle-tracking velocimetric observations in the laboratory of S.-Q. Wang have revealed new phenomenology that is difficult for the tube model to explain.[22−24] On the other hand, accepting its validity, Adams and Olmsted[25] tried to depict the particle tracking velocimetric (PTV) observations with the tube model. In a different but related context, Sussman and Schweizer have suggested in the case of the dynamics of entangled rods that the tube-like confinement is of finite strength[26] and disentanglement can take place in the form of polymer delocalization.[27,28] Because the tube model reduces the dynamics of the entanglement network to a single-chain picture, representing the many-body intermolecular interactions in terms of a tube-like confinement on a test chain, it envisions no barriers against any chain retraction on the Rouse time scale. Consequently, by construction the tube model decouples chain stretching from chain orientation. For example, after a step strain, chain retraction on Rouse time τ_R is followed by chain orientation on the time scale of reptation τ_d. However, experiments by Archer suggested that chain retraction continues to times much longer than the Rouse time.[29]

In this Letter, we report results from computer simulation that aim to explicitly elucidate when chain retraction occurs upon startup shear. We consider shear rate $\dot{\gamma}$ that is higher than the reciprocal reptation time, $1/\tau_d$, but much lower than the reciprocal Rouse time, $1/\tau_R$; i.e., the Weissenberg number Wi =

Received: March 23, 2013
Accepted: May 21, 2013
Published: June 6, 2013

   dx.doi.org/10.1021/mz400145m | ACS Macro Lett. 2013, 2, 561−565

$\dot{\gamma}\tau_d > 1$, and yet the Rouse–Weissenberg number $Wi_R = \dot{\gamma}\tau_R \ll 1$. In this regime, the tube model predicts only orientation of the primitive chain since the degree of chain stretching is given by $Wi_R \ll 1$. In contrast, our Brownian dynamics (BD) simulations show substantial chain stretching and nearly affine deformation on time scales significantly longer than τ_R during startup shear. Furthermore, by a primitive path analysis (PPA), we find that the total number of entanglements decreases over time or elapsed strain. The percentage of initial entanglements decreases even faster. Remarkably, up to many Rouse time τ_R, the decline in the number of initial entanglements during startup shear is slower than that under the quiescent condition, suggesting that the stretched network hinders disentanglement. The rest of this Letter is organized as follows. After a brief review of the theoretical prediction from the tube model concerning the chain dimension as a function of the elapsed strain $\gamma = \dot{\gamma}t$, we present our BD simulation method. Subsequently, we report the simulation results on both the chain conformation and the state of entanglement. We conclude with a discussion of the implications of these results.

According to the tube model,[6] upon startup shear under the condition of $\tau_d^{-1} \ll \dot{\gamma} \ll \tau_R^{-1}$, there would be only chain orientation and no chain stretching; the left half of the inequality indicates that the chain will be oriented due to the tube confinement, while the right half of the inequality ensures that there is little chain stretching since chain relaxation in the tube takes place on times scale of the Rouse time. Without stretching in the contour length of the tube (the primitive chain), the effect of the deformation is a simple reorientation of the unit tangent vector $\vec{u}$ of the primitive chain by the strain tensor $\mathbf{E}$ to $(\mathbf{E}\cdot\vec{u})/|\mathbf{E}\cdot\vec{u}|$, where $\mathbf{E} = (1,\gamma,0;\ 0,1,0;\ 0,0,1)$ for simple shear. This reorientation leaves the overall mean-square radius of gyration $\langle R_g^2\rangle$ unaltered from its equilibrium value $\langle R_{g0}^2\rangle$, while its components are changed to (see Supporting Information).

$$\langle R_{g\alpha}^2\rangle = \langle R_{g0}^2\rangle\langle(\mathbf{E}\cdot\vec{u})_\alpha(\mathbf{E}\cdot\vec{u})_\alpha/|\mathbf{E}\cdot\vec{u}|^2\rangle;\ (\alpha = x, y, z) \quad (1)$$

The average in eq 1 can be written in spherical polar coordinates as angular integrals

$$\begin{cases} \langle R_{gx}^2\rangle = \frac{1}{4\pi}\langle R_{g0}^2\rangle \int_0^{2\pi}[\cos^2\varphi + f(\varphi)]d\varphi \int_0^{\pi} g(\varphi,\theta)d\theta \\ \langle R_{gy}^2\rangle = \frac{1}{4\pi}\langle R_{g0}^2\rangle \int_0^{2\pi}\sin^2\varphi d\varphi \int_0^{\pi} g(\varphi,\theta)d\theta \\ \langle R_{gz}^2\rangle = \frac{1}{4\pi}\langle R_{g0}^2\rangle \int_0^{2\pi} d\varphi \int_0^{\pi} g(\varphi,\theta)\cot^2\theta d\theta \end{cases} \quad (2)$$

where $f(\varphi) = 2\gamma \sin\varphi\cos\varphi + \gamma^2\sin^2\varphi$; $g(\varphi,\theta) = \sin^3\theta/[1 + f(\varphi)\sin^2\theta]$. Results of these integrals do not have analytical forms but can be numerically evaluated. For comparison, we also list the results for the affine deformation. In the case of affine deformation, from $\langle R_{g\alpha}^2\rangle = \langle R_{g0}^2\rangle\langle(\mathbf{E}\cdot\vec{u})_\alpha(\mathbf{E}\cdot\vec{u})_\alpha\rangle$, we have simply

$$\begin{cases} \langle R_{gx}^2\rangle = \frac{1}{3}\langle R_{g0}^2\rangle(1 + \gamma^2) \\ \langle R_{gy}^2\rangle = \langle R_{gz}^2\rangle = \frac{1}{3}\langle R_{g0}^2\rangle \end{cases} \quad (3)$$

We now use computer simulation to test whether $\langle R_{gi}^2\rangle$ follows the tube model prediction in eq2 or conforms more closely to the affine deformation results of eq 3.

Our BD simulations are performed under conditions of fixed temperature and volume. The system consists of 141 chains of uniform length $N = 500$ at a bead density of $\rho = 0.85\sigma^{-3}$. The initial states are prepared by Lattice Monte Carlo (MC)[30] sampling allowing chain crossing, which considerably reduces the time required for system equilibration. We numerically solve the BD equations of motion and further equilibrate the system under BD for a time on the order of τ_d. We generate shear by displacing the upper wall with a fixed velocity $\vec{u}$ in the x-direction relative to the stationary bottom wall. All monomers within a distance less than σ from the two walls are permanently adhered to the walls (to ensure perfect nonslip of the walls). Periodic boundary conditions are only imposed in the x- and z-directions. The simulation box is set at $L_x = L_y = 4R_g$ and $L_z = 3R_g$, where $R_g = \langle R_{g0}^2\rangle^{1/2}$. In the evaluation of the chain conformation and entanglements, all data reported are taken by averaging over 40 independent samples; only nonwall-tethered chains are taken into account (there are about 75 such free chains in each sample).[31]

We use the bead–spring model as in the work of Kremer and Grest.[14] The excluded volume interaction is accounted for by the repulsive part of the Lennard-Jones potential with energy parameter ε and length scale σ, obtained by truncating and shifting the Lennard-Jones potential at the distance cutoff $r_c = 2^{1/6}\sigma$.[14,32] Chain connectivity is modeled by the finitely extensible nonlinear elastic (FENE) potential between adjacent monomers, with a spring constant $k = 30$ in reduced unit, and fully stretched bond length $R_0 = 1.5\sigma$, leading to an average bond length of 0.97σ.[14,32] To fully capture polymer entanglement, it is crucial that bonds do not cross each other. In standard simulation of polymers, crossing is rare except in strongly deformed polymer networks.[32,33] For the large deformations studied in this work, detecting and preventing bond crossings is critical. We follow the approach of Kumar and Larson,[34] who developed a method that uses spring–spring repulsion to prevent the passage of two springs through each other. Here, the spring–spring repulsive potential U_{rep} is chosen as

$$U_{rep} = \begin{cases} 4\varepsilon\left[\left(\frac{\sigma}{2D}\right)^{12} - 1\right]; & D < \sigma/2 \\ 0; & D \geq \sigma/2 \end{cases} \quad (4)$$

where D is the distance of closest approach between two closeby springs. Since BD simulations are carried out by integrating force balances on beads, the repulsive spring force is converted into bead forces by a simple lever rule relation.[34]

Having specified the interaction potentials, the BD equation of motion for bead i is

$$\dot{\vec{r}}_i(t) = -\frac{1}{\mu}\nabla U_i + \frac{1}{\mu}\vec{f}_i(t) \quad (5)$$

Here U_i is the sum of all the interaction potentials discussed above; μ is the friction coefficient; and $\vec{f}_i(t)$ is a random force related to μ by the fluctuation dissipation theorem $\langle\vec{f}_i(t)\vec{f}_j(t')\rangle = 2\mu k_B T\delta_{ij}\delta(t - t')\mathbf{I}$, where $\mathbf{I}$ is the unit tensor. The equations are integrated with a time step $\Delta t = 0.006\tau$, where τ is the unit of time defined as $\tau = (m\sigma^2/\varepsilon)^{1/2}$. We present our results in reduced units in which $\sigma = \varepsilon = m = 1$ and the temperature is $k_BT = 1.0$, and the friction coefficient is taken to be $\mu = 0.5\tau^{-1}$.

For $N = 500$, the chains are well entangled. The Rouse time τ_R is determined from $\tau_R = (1/3\pi^2)\cdot 6\langle R_{g0}^2\rangle/D_R$, where D_R is the Rouse self-diffusion constant, which is obtained by extrapolation of simulation data of nonentangled polymers.[6] To evaluate the terminal relaxation time (reptation or disengagement time, τ_d), we make use of the relation $\tau_d/\tau_R = D_R/D_s$, where D_s is the actual self-diffusion constant.[6] Numerically

dx.doi.org/10.1021/mz400145m | ACS Macro Lett. 2013, 2, 561–565

consistent with the results of Kremer and Grest,[14] we find $\langle R_{g0}^2 \rangle$, D_s, D_R, τ_R, and τ_d are 138, 8.67×10^{-6}, 1.3×10^{-4}, 2.15×10^5, and 3.23×10^6, respectively.[35]

To quantify the evolution of entanglements during deformation, we adopt a PPA introduced by Sukumaran et al.[32] based on Edwards's definition of a primitive path. At any given time, we freeze the conformation of all the chains in the system and apply the PPA to examine the number of chain strands that hinders the lateral motion of a test chain. This number is averaged over all chains and is defined as the number of entanglements per chain. We follow the time dependence of this quantity normalized by its value at equilibrium, as a means to gauge how the deformation alters the topological interactions in the entangled polymer melt.

Unlike macroscopic experiments, computer simulation provides direct information on the molecular conformation of the chains during startup shear. In Figure 1 we show snapshots

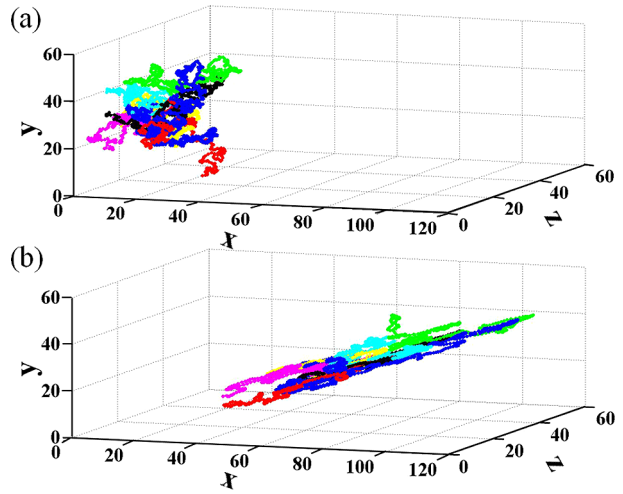

Figure 1. Snapshots of several representative chains in the entangled melts. (a) At equilibrium. (b) At 200% strain during startup shear under the condition of $Wi_R = 1/6$.

of several representative chains in the middle of the simulation box before and during shear. The comparison between Figure 1(a) and 1(b) clearly indicates significant chain stretching and alignment in the XY plane. On the other hand, the chain conformation appears relatively isotropic in the YZ plane. In this Letter, we fix the shear rate at $(6\tau_R)^{-1}$, so that a shear strain of 200% takes $12\tau_R \gg \tau_R$. The corresponding Weissenberg number $Wi = \dot{\gamma}\tau_d$ is between 2.5 and 3.5 depending on the definition of the reptation time used. We have verified that at this shear rate the actual velocity profile varies linearly in the gradient direction at all stages of the simulation. Because chain retraction takes place on the time scale of order τ_R, the tube model would predict no significant increase in chain stretching beyond a strain of 1/6. We have also performed simulations with strain rates $(8\tau_R)^{-1}$ and $(4\tau_R)^{-1}$; the results are qualitatively similar.

We quantify the information contained in Figure 1 by measuring the mean square radius of gyration $\langle R_g^2 \rangle$ as a function of the elapsed strain γ during the startup shear; the results are shown in Figure 2. Up to a strain of 1.5, the increase in $\langle R_g^2 \rangle$ follows closely the behavior expected of affine deformation. In contrast, the tube model predicts a negligible increase in $\langle R_g^2 \rangle$. At higher shear strains, the increase of the overall coil size slows down, deviating downward from the affine deformation limit.

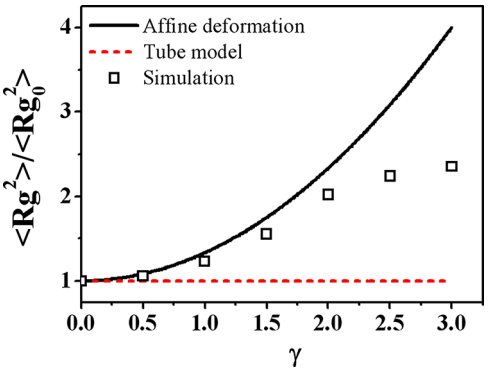

Figure 2. Comparison of stretching factor of the mean square radius of gyration of the entangled polymer chains during startup shear under the condition of $Wi_R = 1/6$ from the simulation relative to the affine deformation depiction and the prediction of the tube model.

Before presenting additional information to shed light on why the coil size ceases to increase affinely at larger strains, we analyze the projections of the chain conformation parallel and perpendicular to the shearing direction. Figure 3 shows more

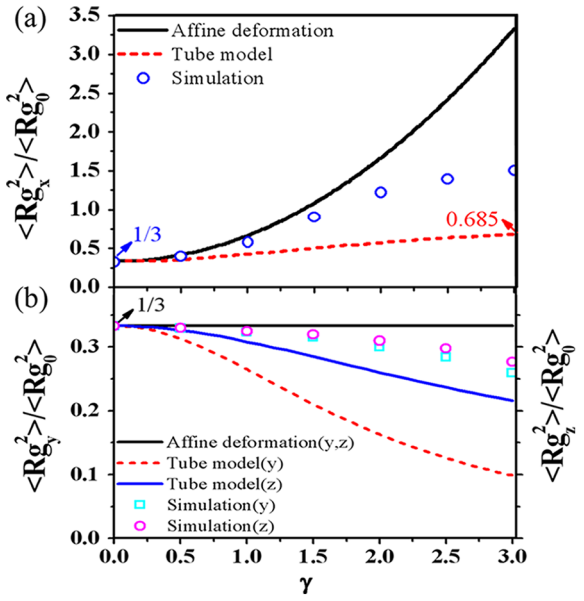

Figure 3. Components of the gyration tensor of the entangled polymer chains. (a) The x-component. (b) The y- and z-components.

detailed information on the chain deformation during the startup shear. These results confirm that the chain deformation is approximately depicted by the limit of affine deformation up to a shear strain of $\gamma = 2$. It is interesting to note that the tube model depicts very different projections along the velocity gradient and the vorticity directions as shown, respectively, by the dashed and continuous curves in Figure 3(b). In contrast, the simulation data show surprisingly little difference between $\langle R_{gy}^2 \rangle$ and $\langle R_{gz}^2 \rangle$, conforming closely to the depiction based on affine deformation.

Our computer experiments also yield insight into how to define chain entanglement and how to follow its evolution during startup shear. Such questions are intimately related to another set of important questions: (a) when does an entangled polymer cease to deform affinely, and (b) how does chain disentanglement occur? Specifically, why and how does chain

dx.doi.org/10.1021/mz400145m | ACS Macro Lett. 2013, 2, 561−565

deformation eventually become nonaffine as seen in Figures 2 and 3? The analysis shown in Figure 4 gives us some idea.

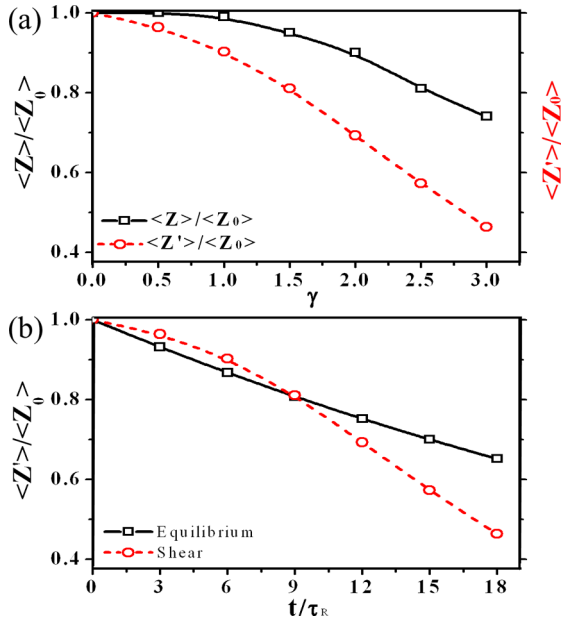

Figure 4. Average number of entanglements as a function of (a) shear strain γ or (b) time t/τ_R during startup shear. Note that $\langle Z_0 \rangle$ and $\langle Z \rangle$ are the number of entanglements per chain in equilibrium and during shear, respectively. $\langle Z' \rangle$ is the number of surviving initial entanglements per chain.

Plotted in Figure 4(a) are two sets of data, one indicating the percentage of the initial entanglements (per chain) that survive at the various stages during the startup shear and the other showing the overall amount of entanglements normalized by the number Z_0 of entanglements per chain in equilibrium. Unlike previous computer simulations that evaluate chain entanglement by PPA indiscriminatively, our analysis differentiates new from old entanglements by keeping track of which surrounding chains form entanglement (as defined by PPA) with a given test chain. In passing, we note that such quantification of chain entanglement as shown in Figure 4(a) is not available within the tube model framework. The tube model does not even address the question of whether and how the lack of affine deformation beyond τ_R amounts to chain disentanglement since the tube confinement is always perceived to be present.

It is not surprising that the increase of the overall coil size could initially be depicted by affine deformation, although some original entanglements have been replaced by new ones. However, as the overall level of chain entanglement decreases, the molecular deformation becomes more nonaffine as shown in Figures 2 and 3. In other words, the downward deviation of the squares from the continuous curve of affine deformation in Figure 2 directly correlates with the loss of chain entanglement depicted by the squares in Figure 4(a). Finally, we compare the loss of the original entanglements over time during the startup shear with that in quiescence due to the chain diffusion in Figure 4(b). Remarkably, we see that the initial entanglements disappear faster in quiescence than in shear. Our interpretation is that the initial affine deformation of the entanglement network actually tightens up the intermolecular coupling and makes it more difficult to lose entanglement relative to the loss of entanglements by diffusion in quiescence. In the later stage the startup shear does accelerate the disappearance of the original entanglements relative to the renewal rate in quiescence, reflecting the effect of convection.

Our BD simulations have revealed remarkable clues about chain entanglement in the presence of startup shear. Figures 1−4 show that even for a rather small Rouse−Weissenberg number $Wi_R = 1/6$ a chain undergoes considerable stretching well past the Rouse time. In other words, the chains continue to deform in a quasi-affine manner, suggesting that the construction of the tube model is unrealistic. Indeed, the smoothed-out description of intermolecular coupling in entangled polymers by a tube has difficulty in both identifying and quantifying chain entanglements. In other words, unable to explicitly account for the active role of intermolecular interactions in the description of polymer entanglement, the tube model could only envision chain retraction leading to unrealistically reduced chain dimensions.

In conclusion, chain entanglement actually involves active localized intermolecular interactions that may be perceived as network junctions. To describe its dynamic evolution, we have to keep track of the removal and reformation of these intermolecular coupling junctions, which is often popularly known as *entanglement points*. A realistic theoretical description of polymer entanglement under large deformation has to characterize the dynamics of these entanglement points and to address the fundamental question of when the chain deformation ceases to be affine and when the system starts to yield, i.e., to transition from dominantly elastic deformation to massive irrecoverable deformation. Our computer experiments reveal significant chain stretching during a startup shear even at such low rates where the tube model anticipates only chain orientation. Thus, the present simulation results are starkly inconsistent with the Rouse retraction dynamics of the tube model and question the apparent agreement between the theory and experiment concerning the nonlinear rheology of entangled polymers.

The present work is only the first step toward probing a realistic theoretical framework for dynamics of entangled polymers under large deformation. There are several key questions that remain to be addressed. One of the most important is how evolution of chain conformation and entanglements produce the corresponding stress, i.e., what the true molecular picture is for stress overshoot upon startup shear at various rates for both $Wi_R < 1$ and $Wi_R > 1$, and what molecular processes give rise to the strain softening during stress relaxation from a large step strain. We will take up these questions in forthcoming investigations.

■ ASSOCIATED CONTENT

Ⓢ Supporting Information

A detailed derivation demonstrating that, under the assumptions of the tube model, the mean-square radius of gyration and the mean-square end-to-end distance remain unchanged from their equilibrium value, while their components are given by eq 1, for the flow condition considered in our work. This material is available free of charge via the Internet at http://pubs.acs.org.

■ AUTHOR INFORMATION

Corresponding Author

*E-mail: ljan@ciac.jl.cn; swang@uakron.edu; zgw@caltech.edu.

Notes

The authors declare no competing financial interest.

■ ACKNOWLEDGMENTS

This work is supported, in part, by the National Natural Science Foundation of China (No. 21120102037) and further subsidized by the Special Funds for National Basic Research Program of China (No. 2012CB821500). S.Q.W. acknowledges support from the US National Science Foundation (DMR-0821697 and DMR-1105135).

■ REFERENCES

(1) Green, M. S.; Tobolsky, A. V. *J. Chem. Phys.* **1946**, *14*, 80.
(2) Lodge, A. S. *Elastic Liquids*; Academic Press: London, 1964.
(3) Astarita, G.; Marrucci, G. *Principles of Non-Newtonian Fluid Mechanics*; McGraw-Hill Inc.: US, 1974.
(4) Bird, R. B.; Armstrong, R. C.; Hassager, O. *Dynamics of Polymeric Liquids*; Wiley: New York, 1987.
(5) Kaye, A. *Non-Newtonian Flow in Incompressible Fluids*; College of Aeronautics: Cranford, U. K., 1962.
(6) Doi, M.; Edwards, S. F. *The Theory of Polymer Dynamics*; Clarendon: New York, 1986.
(7) de Gennes, P. G. *Scaling Concepts in Polymer Physics*; Cornell University: Ithaca, 1979.
(8) Rubinstein, M.; Colby, R. H. *Polymer Physics*; Oxford University: Oxford, 2003.
(9) Mcleish, T. C. B. *Adv. Phys.* **2002**, *51*, 1379.
(10) Morse, D. C. *Phys. Rev. E* **2001**, *63*, 031502.
(11) Bent, J.; et al. *Science* **2003**, *301*, 1691.
(12) Schleger, P.; Farago, B.; Lartigue, C.; Kollmar, A.; Richter, D. *Phys. Rev. Lett.* **1998**, *81*, 124.
(13) Ebert, U.; Baumgärtner, A.; Schäfer, L. *Phys. Rev. Lett.* **1997**, *78*, 1592.
(14) Kremer, K.; Grest, G. S. *J. Chem. Phys.* **1990**, *92*, 5057.
(15) Kremer, K.; Grest, G. S.; Carmesin, I. *Phys. Rev. Lett.* **1988**, *61*, 566.
(16) Smith, S. W.; Hall, C. K.; Freeman, B. D. *Phys. Rev. Lett.* **1995**, *75*, 1316.
(17) Kröger, M.; Hess, S. *Phys. Rev. Lett.* **2000**, *85*, 1128.
(18) Qin, J.; Milner, S. T.; Stephanou, P. S.; Mavrantzas, V. G. *J. Rheol.* **2012**, *56*, 707.
(19) Larson, R. G. *J. Polym. Sci., Part B: Polym. Phys.* **2007**, *45*, 3240.
(20) Likhtman, A. E. *J. Non-Newtonian Fluid Mech.* **2009**, *157*, 158.
(21) Likhtman, A. E.; Sukumaran, S. K.; Ramirez, J. *Macromolecules* **2007**, *40*, 6748.
(22) Wang, S. Q. *Phys. Rev. Lett.* **2006**, *97*, 187801.
(23) Wang, S. Q.; Ravindranath, S.; Wang, Y. Y.; Boukany, P. E. *J. Chem. Phys.* **2007**, *127*, 064903.
(24) Wang, Y. Y.; Wang, S. Q. *J. Rheol.* **2009**, *53*, 1389.
(25) Adams, J. M.; Olmsted, P. D. *Phys. Rev. Lett.* **2009**, *102*, 067801.
(26) Sussman, D. M.; Schweizer, K. S. *Phys. Rev. Lett.* **2011**, *107*, 078102.
(27) Sussman, D. M.; Schweizer, K. S. *J. Chem. Phys.* **2011**, *135*, 131104.
(28) Sussman, D. M.; Schweizer, K. S. *Macromolecules* **2012**, *45*, 3270.
(29) Archer, L. A. *J. Rheol.* **1999**, *43*, 1555.
(30) Shaffer, J. S. *J. Chem. Phys.* **1994**, *101*, 4205.
(31) For the chains that we used to collect the data (the nonwall-tethered chains) in our simulation, we have examined their conformation and did not find any significant effects of the confining wall. However, constraint of the wall may affect the free chains to some degree due to possible existence of permanent loops near the wall. To address this concern, we have compared the results from the chains in the middle of the box with those free chains next to the surfaces. The comparison indicates that effect of proximity to the wall is small.
(32) Sukumaran, S. K.; Grest, G. S.; Kremer, K.; Everaers, R. *J. Polym. Sci., Part B: Polym. Phys.* **2005**, *42*, 917.
(33) Everaers, R.; Kremer, K. *J. Mol. Model.* **1996**, *2*, 293.
(34) Kumar, S.; Larson, R. G. *J. Chem. Phys.* **2001**, *114*, 6937.
(35) We have also estimated the Rouse time and the reputation time by the location of the crossover in the monomer mean-square displacement, with the result $\tau_R = 2.3 \times 10^5$ and $\tau_d = 4.1 \times 10^6$, respectively.